Simulated Contrast Performance of Phase Induced Amplitude Apodization (PIAA) Coronagraph Testbed

Erkin Sidick*[a], Brian Kern[a], Ruslan Belikov[b], Andreas Kuhnert[a], and Stuart Shaklan[a]
[a]Jet Propulsion Laboratory, California Institute of Technology, 4800 Oak Grove Drive, Pasadena, CA 91109, USA
[b]NASA Ames Research Center, Moffett Field, CA 94035, USA

ABSTRACT

We evaluate the broadband contrast performance of a Phase Induced Amplitude Apodization (PIAA) coronagraph configuration through modeling and simulations. Broadband occulter mask design for PIAA-CMC is at an early stage, and a study of the effects of wavefront control on broadband contrast is needed to determine the level of control the occulting mask must achieve, so that the combination of occulter and wavefront control optimization meets contrast targets. The basic optical design of the PIAA coronagraph is the same as NASA's High Contrast Imaging Testbed (HCIT) setup at the Jet Propulsion Laboratory (JPL). Using two deformable mirrors and a broadband wavefront sensing and control algorithm, we create a "dark hole" in the broadband point-spread function (PSF) with an inner working angle (IWA) of $2(f\lambda/D)_{sky}$. We evaluate a system using PIAA mirrors to create an apodization but not having any wavefront error at its exit-pupil, and having an obscured pupil and a new, 20-ring PIAACMC occulting mask. We also investigate the effect of Lyot stops of various sizes. For the configuration simulated here with the second-generation PIAA mirrors and early mask designs (which were not yet fully optimized), the best 10% broadband contrast value was $\sim 6.1\times10^{-8}$. This is a 2x improvement beyond what the coronagraph produces in the absence of wavefront control, which implies that further improvement must come from architecture changes or further mask optimization improvements.

Key words: Coronagraphy, adaptive optics, space telescopes, exoplanets

INTRODUCTION

One of the important milestones of the Phase Induced Amplitude Apodization (PIAA) coronagraph, one of NASA's High Contrast Imaging Testbed (HCIT) setups at the Jet Propulsion Laboratory (JPL), is to achieve 10^{-9} mean contrast in a dark hole with a 10% broadband light. So far a mean intensity of $5\text{x}10^{-10}$ has been achieved experimentally in a dark hole in the monochromatic point-spread function (PSF) with an IWA of $2(f\lambda/D)_{sky}$ using a configuration in which a DM was placed downstream of the front end PIAA set. The first-generation aspheric PIAA mirrors used in that experiment were made by Axsys and are identified as "PIAA-1" in this paper. They are described in detail in Ref. 1. Placing the DM upstream of the front end PIAA sub-system enables the correction of high spatial frequencies before the PIAA remapping carries that information to frequencies higher than Nyquist frequency, allowing a larger outer working angle (OWA). Also, using an inverse-PIAA set at the back end enables one to recover a sharp diffraction-limited image over a useful field of view [2-3]. In a previous report we compared the broadband-contrast performance of several PIAA coronagraph configurations using PIAA-1 mirrors through modeling and simulations [4].

The new PIAA configuration currently implemented on the HCIT uses the second-generation PIAA mirrors fabricated by Tinsley and are identified as "PIAA-2" in this paper. The new system also uses two 32x32 actuator DM's, and a new (but not yet fully optimized) 20-ring PIAACMC occulting mask. In this report, we evaluate the broadband contrast performance of this new PIAA coronagraph system, and examine the effect of Lyot stops of various sizes with an obscuration present. The goal of this investigation is to determine, for a given target contrast (typically 10^{-8} to 10^{-9}), how much optimization must be done on the mask so that, when the occulting mask and wavefront control are combined, the system reaches the target contrast. In other coronagraphs, the effect of wavefront control on broadband contrast ranges from none (for an achromatic coronagraph) to over two orders of magnitude of improvement.

---

*Erkin.Sidick@jpl.nasa.gov; Phone 1 818 393-7585; Fax 1 818 393-9471; www.jpl.nasa.gov

Space Telescopes and Instrumentation 2014: Optical, Infrared, and Millimeter Wave, edited by Jacobus M. Oschmann, Jr., Mark Clampin, Giovanni G. Fazio, Howard A. MacEwen, Proc. of SPIE Vol. 9143, 91430W · © 2014 SPIE
CCC code: 0277-786X/14/$18 · doi: 10.1117/12.2055006

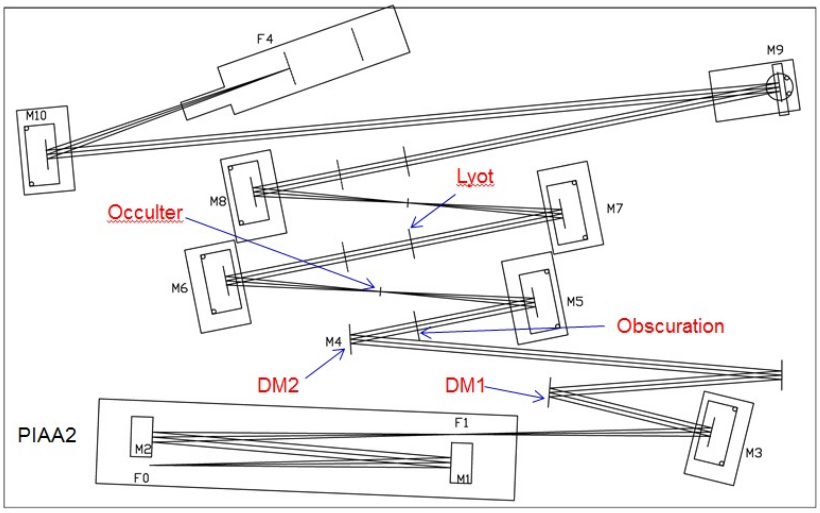

Fig.1. Layout of optics on table, to scale. The source is at the bottom-right (F0). M9 is a flat mirror.

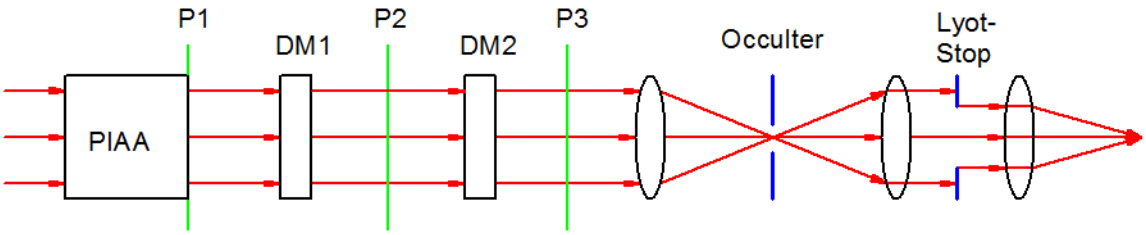

Fig.2. Propagation sequence to the science camera, not to scale. This is the optical configuration modeled in this paper. The planes conjugate to the pupil stop (P1) are labeled as P2, P3 and Lyot-Stop.

BACKGROUND

1.1 PIAA Implementation on HCIT

The PIAA-2 mirrors in this paper were used previously on HCIT [5] and at NASA Ames [6]. The PIAA experiment at HCIT is laid out on a 5'x8' optical table, in a vacuum chamber. The coronagraph uses several off-axis parabolas (OAPs) as relay optics. In the collimated beam after the DMs there is an obscuration mask, which produces a central obscuration and four "cross-hair" spiders. The obscuration mask projects geometrically to a 23 actuator diameter circle on each DM (out of the full 32x32 actuators on each DM). The light is brought to a focus where the occulter is located, then recollimated to pass through a Lyot stop, and imaged onto a CCD camera. A sketch of the layout is shown in Figs. 1 and 2. In Fig. 2, the three pupil-planes, P1-P3, indicate the same plane marked as "Obscuration" in Fig. 1, as explained later in this section.

1.2 Amplitude at the Exit-Pupil

In this paper, we use a PIAA output amplitude similar to that of the PIAA-2 mirrors alone (truncated at a radius smaller compared to their clear aperture), but with a small modification to bring them to a PIAACMC (PIAA complex-mask coronagraph) apodization appropriate to the occulter described in the next section. This amplitude modification is created by the two DMs, using about 150 nm of stroke, but is treated as the "starting point" of the DM solution and simulation. This treatment is chosen to enable testbed validation using the existing PIAA-2 mirrors. The output amplitude of PIAA-2 mirrors is multiplied by an obscuration mask, and this will serve as the starting point for the simulations in the next section. No other optical aberration is included in the simulations. On the testbed, the obscuration is introduced at the plane marked as "Obscuration" in Fig. 1, or as "P3" in Fig. 2. For simulations, we

multiplied the PIAA-2 output amplitude with the obscuration mask at "P1" in Fig. 2 rather than "P3," for simplicity (the difference should be minimal).

The nominal Lyot stop is identical to the obscuration mask. We will also simulate Lyot stops with other 2 sizes. One has an opening 1pix smaller at all edges, and the other one is 3pix smaller.

1.3 Occulter

The PIAACMC apodization "ideal" design uses a circular, real-valued, and partially transmitting occulter whose outer diameter is $r = 1.6 f(\lambda / D)_{\text{sys}} = 25.74\mu\text{m}$ and complex amplitude transmission $t = -0.28$, where the subscript "sys" means "system" and denotes corresponding location in the occulter plane or the camera at the final focal plane. Two difficulties arise in fabricating such an occulter: the material must produce both attenuation and a 180-degree phase shift, and the radius must scale with wavelength. The fabrication path chosen for testbed validation is to use a sequence of dielectric annuli (PMGI, $T = 1$). Its surface profile is like a diffraction grating, so less light ends up inside the Lyot stop. Because the rings have a phase-only effect, which depends linearly on wavelength (ignoring dispersion), a broadband optimization can produce a mask that performs well over finite bandwidths. A 20-ring occulter was designed with a (preliminary and not yet fully tuned) broadband optimization for this study. We will also examine the monochromatic contrast performance of 5-ring, 10-ring and 15-ring occulters as well, although these occulters were designed monochromatically, and so are not expected to perform well over a finite bandwidth.

As explained in Ref. 4, the PIAA mirrors apodize the pupil amplitude and distort the phase map of the input pupil. At the same time, they produce a magnification and aberration of off-axis sources, which depends on the details of the apodization and stops. For the optical configuration in Fig. 1, this magnification is 1.2:

$$(\lambda / D)_{\text{sys}} = 1.2 \times (\lambda / D)_{\text{sky}}, \tag{1}$$

where the "sky" subscript denotes corresponding locations in the source plane.

1.4 Definitions of Dark-Hole Areas and Contrast

For the current optical system with two DM's, we carry out wavefront control (WFC) or electric-field conjugation (EFC) over a region Ω_c, where Ω_c is a full dark-hole region extending from a circular shape at the center to a square-shaped outer boundary. In this paper, the Ω_c has a boundary defined by $[R_{\min}, X_{\max}] = [r_{\min}, x_{\max}] / f = [1.9, 5.1](\lambda / D)_{\text{sky}}$, where f is a focal length. We will evaluate the performance of the PIAA coronagraph using the mean normalized intensity or mean contrast, C_b, defined as

$$C_b = Mean\{I(x,y) / I_0\}_{(x,y)\in\Omega_b}, \tag{2}$$

where "Mean" represents a mean-value operation, $I(x,y)$ is the image intensity of the occulted star, I_0 is the peak value of the unocculted star intensity, and Ω_b represents the contrast dark-hole area. The subscript "b" means "big" and is used here to have the same naming convention as in our previous publications [7]. In this paper, the boundary of the Ω_b is defined by $[R_{\min}, X_{\min}] = [2, 5](\lambda / D)_{\text{sky}}$. That is, we have chosen an Ω_b slightly smaller than the corresponding Ω_c in this study. We will keep the values of $[R_{\min}, X_{\min}]$ unchanged for both Ω_c and Ω_b in this report.

1.5 About the Wavefront Control (WFC) Algorithm

In this paper, we use a control algorithm similar to the "minimum-wavefront and optimal control compensator" described in detail in Ref. 8. This approach is also called "Actuator regularization" [9]. The WFC algorithm described in Ref. 8 uses the wavefront at the system exit pupil as its input, and calculate the actuator commands as its output. In the present case we set the DM actuators to superpose the negative of the electric-field (e-field) onto the image plane, with a goal to make the image intensity zero on the region Ω_c on the image plane. Therefore, the WFC algorithm uses an e-field column-vector $\vec{\mathbf{e}}$ as its input, where

$$\vec{\mathbf{e}} = \begin{bmatrix} \Re(\vec{\mathbf{E}}) \\ \Im(\vec{\mathbf{E}}) \end{bmatrix}. \tag{3}$$

The joint cost function now becomes as

$$J = \frac{1}{2}\left(\vec{\mathbf{e}}^T\vec{\mathbf{e}} + \gamma_{\text{wu}}\vec{\mathbf{u}}^T\vec{\mathbf{u}}\right), \tag{4}$$

and the gain matrix $\widetilde{\mathbf{G}}$ is obtained from

$$\widetilde{\mathbf{G}} = \left[\widetilde{\mathbf{S}}^T\widetilde{\mathbf{S}} + \gamma_{\text{wu}}\widetilde{\mathbf{I}}\right]^{-1}\widetilde{\mathbf{S}}^T, \tag{5}$$

where $\widetilde{\mathbf{I}}$ is an identity matrix and $\vec{\mathbf{u}}$ is the DM actuator command vector to be determined. It is obtained from $\vec{\mathbf{u}} = -\widetilde{\mathbf{G}}\vec{\mathbf{e}}_{\text{test}}$, where $\vec{\mathbf{e}}_{\text{test}}$ is the vector of the e-field to be minimized. In Eq. (3), $\vec{\mathbf{E}}$ is the column-vector of the complex e-field on region Ω_c. It is formed by stacking the elements of the complex e-field on region Ω_c in a certain order, as was explained in Eq. (1) of Ref. 8. The $\Re(\vec{\mathbf{E}})$ and the $\Im(\vec{\mathbf{E}})$ are the real and the imaginary parts of $\vec{\mathbf{E}}$, respectively. In Eq. (5), the $\widetilde{\mathbf{S}}$ is the sensitivity matrix consisting of the influence functions of all actuators, and γ_{wu} is the actuator regularization factor. Our Fast Fourier-Transform (FFT) based simulation tool calculates the complex e-field at the final focal plane directly. Therefore, the e-field estimation step [9] is not needed in our simulations. The simulation creates a 1024x1024 pixels (pix) PSF image in the final focal plane, with ~2.13pix per $(\lambda/D)_{\text{sky}}$. There are a total of 2x1024=2048 DM actuators (32x32 actuators x2) in the current 2-DM system, but we exclude the actuators with zero or very weak influences (e.g., outside the 24-actuator diameter of the obscuration mask), thus reducing the number of the actuators used to <2048.

In this report, we carry out broadband control using four wavelengths: λ_1 = 770nm, λ_2 = 790nm, λ_3 = 810nm, and λ_4 = 830nm. This is equivalent to simulating a broadband light with $\Delta\lambda/\lambda_0$ = 10%, where $\Delta\lambda$ is the bandwidth of the propagating beam and λ_0=800nm. For broadband WFC, the e-field column-vector in Eqn. (2) is replaced with [9]

$$\vec{\mathbf{e}} = \begin{bmatrix} \vec{\mathbf{e}}(\lambda_1) \\ \vec{\mathbf{e}}(\lambda_2) \\ \vec{\mathbf{e}}(\lambda_3) \\ \vec{\mathbf{e}}(\lambda_4) \end{bmatrix}. \tag{6}$$

To obtain a broadband PSF, we calculate the PSF intensities at the above four individual wavelengths first, then take their arithmetic average with an equal weight.

SIMULATION RESULTS

1.6 Monochromatic Contrast

We first carried out monochromatic wavefront control as a baseline at each of the four different wavelengths individually with the nominal Lyot stop: 770, 790, 810 and 830nm. Figures 3(a-b) show the before-control and after-

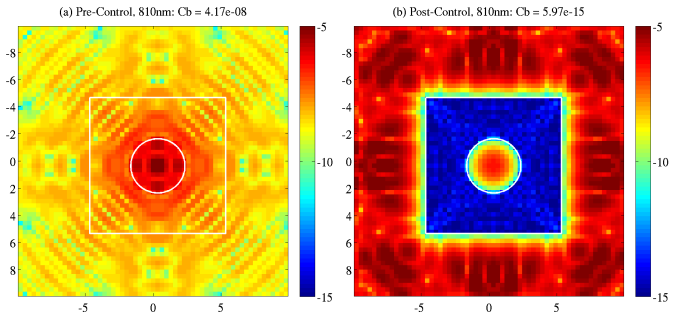

Fig.3. (a) Before-control contrast map, and (b) after control contrast-map at the wavelength of λ = 810nm. The *x*- and the *y*-axes are in $(\lambda/D)_{\text{sky}}$. The white-colored frames show the boundaries of the control dark-hole region, Ω_c.

control contrast maps (or normalized PSF's) at the wavelength of λ = 810nm. They are shown here as an example of monochromatic control results. In this case, the pre-control $C_b = 4.17\times10^{-8}$, and post-control $C_b = 5.97\times10^{-15}$. That is, the contrast floor approaches to numerical noise-floor in this case. The monochromatic control efficiency (the ratio of beginning to ending contrast, i.e., the improvement due to wavefront control) is shown in Fig. 4(a), where the C_b -values are shown as a function of control iteration number for four different wavelengths. The value of the actuator regularization factor, γ_{wu}, is increased four times during the iteration sequence by x10, after control iteration number 4, 9, 14 and 19, and most of the time the increase in γ_{wu} –value resulted in a sharp decrease in C_b -value. Going to less aggressiveness in terms of γ_{wu} –value during a control when the C_b -value stops improving has been our approach in coronagraph control simulations for some time, and worked well most of the time. Figure 4(b) shows before- and after-control C_b -values as a function of control wavelength. The 20-ring occulter used in this simulation was optimized for a center-wavelength of 808nm. But it yields the best before-control and after-control C_b -values at 790nm in Fig. 4(b). This has something to do with the wavelength dependence of the contrast map morphology as will be discussed next.

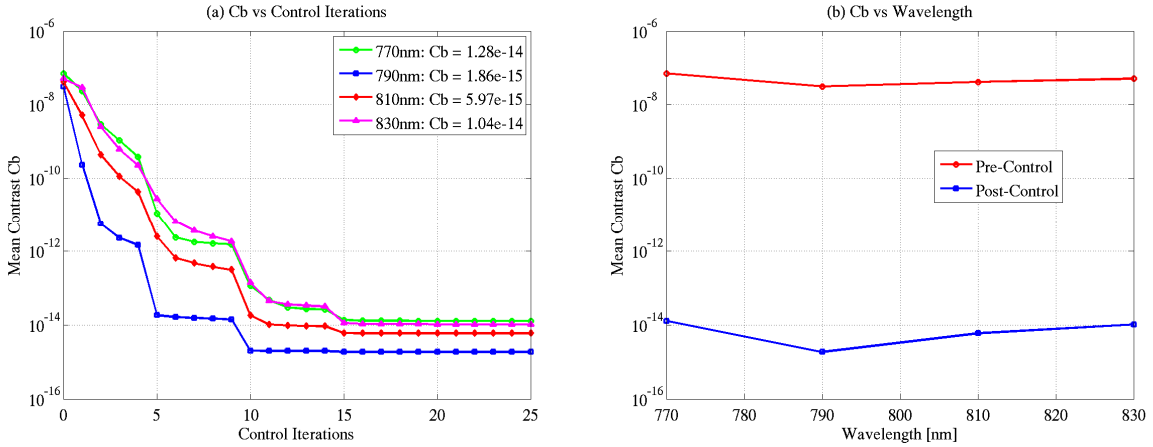

Fig.4. (a) The change in mean contrast, C_b, as a function of control iterations for four different wavelengths. The sharp decreases in C_b –values after control iteration numbers 4, 9, 14, and 19 take place when the actuator regularization factor γ_{wu} is increased by x10 from its current value. (b) Pre- and post-control mean contrast values, C_b, as a function of wavelength.

1.7 Broadband Contrast

The before-control contrast maps at four different wavelengths, 770, 790, 810 and 830nm, and their mean are shown in Fig. 5(a). The corresponding C_b –values are listed in the *x*-label of the same plot. The image of each contrast map extends from -10 to +10$(\lambda/D)_{sky}$ in both *x* and *y*. We note that the morphology of the central $R \sim 5\ (\lambda/D)_{sky}$ part of the PSF images corresponding to the four different wavelengths are very different from each other. This poses a great challenge for broadband wavefront control, as shown in Fig. 5(b), where the after-control contrast maps at the 4 different wavelengths and their mean are shown in the same form as part (a). The before-control to after-control–ratios are [1.9 4.4 3.0 2.0 2.3], respectively for the four individual wavelengths and for their mean. The control efficiency is the best at λ = 790nm and the worst at λ = 770nm.

Another case we considered is to perform monochromatic control at the center-wavelength of λ = 800nm and evaluate the obtained DM solutions with 10%-broadband light. The results are shown in Fig. 5(c). As expected, the broadband C_b –value is worse in this case than the broadband control one, and the difference is about a factor of 2, $C_b = 4.14\times10^{-8}$ versus $C_b = 2.17\times10^{-8}$. The corresponding mean contrast versus control iteration results are shown in Fig. 6(a), and the mean contrast versus wavelength results are shown in Fig. 6(b). In Fig. 6(a), the several sharp

decreases in the monochromatic-control C_b –value (red-curve) takes place when the γ_{wu} –value is increased by a factor of 10 relative to its current value.

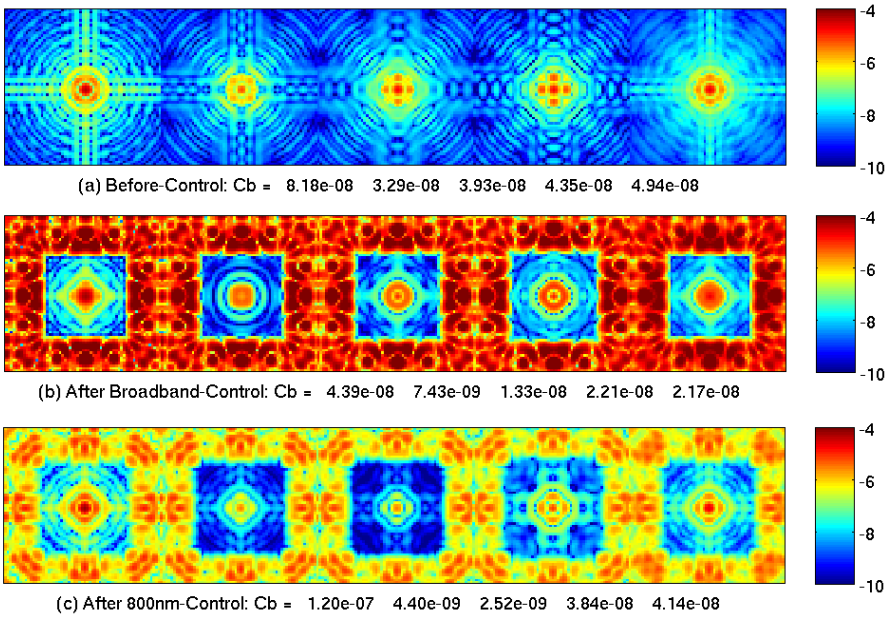

Fig.5. Simulation testing whether it is sufficient to design PIAACMC coronagraph for 1e-7 contrast (allowing very simple manufacture and fast optimization), and rely on wavefront control to dig deeper. Shown are contrast maps at four individual wavelengths, 770, 790, 810 and 830nm, and their mean. (a) Before-control, (b) after broadband-control, and (c) after monochromatic-control at wavelength λ = 800nm. The x-label of each panel lists the C_b –values at the four different wavelengths and that corresponding to 10%-broadband. Panel (c) shows the results of a case where the control is carried out with a monochromatic, central-wavelength of λ = 800nm and obtained DM commands are evaluated at 10%-broadband. The image corresponding to each wavelength extends from -10 to +10 $(\lambda/D)_{sky}$ in both *x* and *y*.

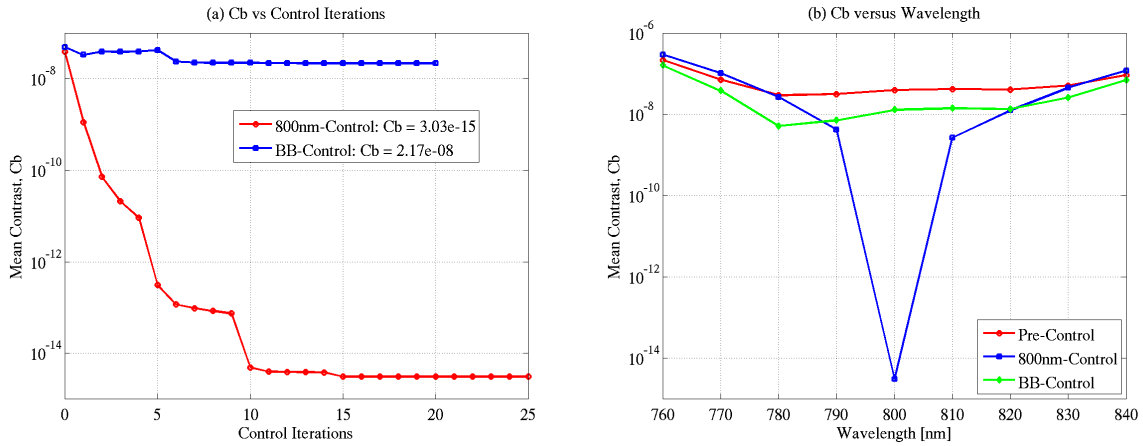

Fig. 6. (a) C_b –value as a function of control iteration number. The red-curve corresponds to a monochromatic control at λ = 800nm, evaluated only at 800 nm, and the blue-curve to a 10%-broadband control. (b) Before- and after-control C_b –values as a function of wavelength. The three curves correspond to the 3 cases shown in Figs. 5(a-c). For these tests, PIAACMC masks were intentionally designed for the less aggressive 1e-7 contrasts to achieve greater shape simplicity and test whether the wavefront control system can dig deeper, essentially acting as part of the coronagraph.

1.8 Lyot Stops of Different Sizes

We have also examined the effects of the Lyot stops having different sizes on the broadband contrast, by carrying-out the control inside a half-dark region, that is, inside Ω_c having $x > 0$. We considered three cases for the size of Lyot stop: Nominal, 1pix smaller opening, and 3pix smaller opening, respectively. Here, the word "1pix smaller" refers to a Lyot stop whose clear aperture is reduced by 1pix at all of its edges. The results of broadband C_b –value versus control iteration number are shown in Fig. 7, where the result of the full-dark hole broadband control is also included as a reference. Overall, the half-dark hole control gives better C_b –value than the full-dark hole control, by approximately a factor of 2 with the nominal (0pix) Lyot stop opening. Also, the C_b –value gets worse as the Lyot stop opening gets smaller, by 24% when the Lyot stop opening is the smallest. Figures 8(a-b) show the before- and the after-control contrast maps. Here, we provided both the before- and the after-control contrast maps corresponding to the smallest Lyot stop opening (3pix) as an example. The before-control contrast maps are included here as a comparison to the post-control ones.

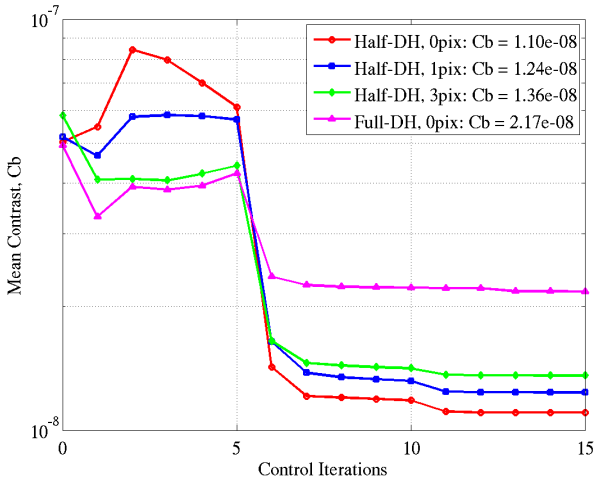

Fig.7. Broadband C_b –value as a function of control iteration number. The acronym "DH" means "dark-hole" and the *n* in "*n*pix" shows the number of pixels by which the clear aperture of the Lyot stop is reduced. The purple-curve is the same as the blue-curve in Fig. 6(a) and is included here as a reference.

1.9 Performance of 5-Ring, 10-Ring, and 15-Ring Occulters

We have also designed 5-ring, 10-ring and 15-ring occulting masks using only monochromatic considerations (i.e., optimized only at a single wavelength), and evaluated their monochromatic contrast performance at λ = 810nm. Figures 9(a-c) show the before control contrast maps, and Figs. 9(d-f) show the after-control contrast maps. As expected, the after-control C_b –value improves with increased ring numbers, and it approaches to the numerical noise-floor in the case of 15-ring occulter. For these 3 cases the before-control broadband mean contrast values are 6.78E-6, 2.62E-6, and 1.49E-6, and the resulting after-control broadband mean contrast values are 3.93E-6, 2.03E-6, and 1.06E-6, respectively. That is, the improvement in the broadband mean contrast is very small in all of these three cases.

4. CONCLUSION

One of the important milestones of the PIAA coronagraph project is to demonstrate 1×10^{-9} contrast with 10% bandwidth. In order to identify the potentials and the limitations of a 2-DM PIAA coronagraph on HCIT built with obscuration, we have evaluated through modeling and simulations the broadband contrast performance of a PIAA coronagraph using a 20-ring broadband occulting mask. We found that the PSF morphology exhibits a strong dependence on wavelength, and broadband control does not result in contrast improvement beyond a factor of 2.3 in the case of a full dark-hole. In our simulations, the 10%-broadband mean contrast improved from a pre-control value of 4.94E-8 to 2.17E-8 after broadband control. When the control was carried-out at a monochromatic central-wavelength

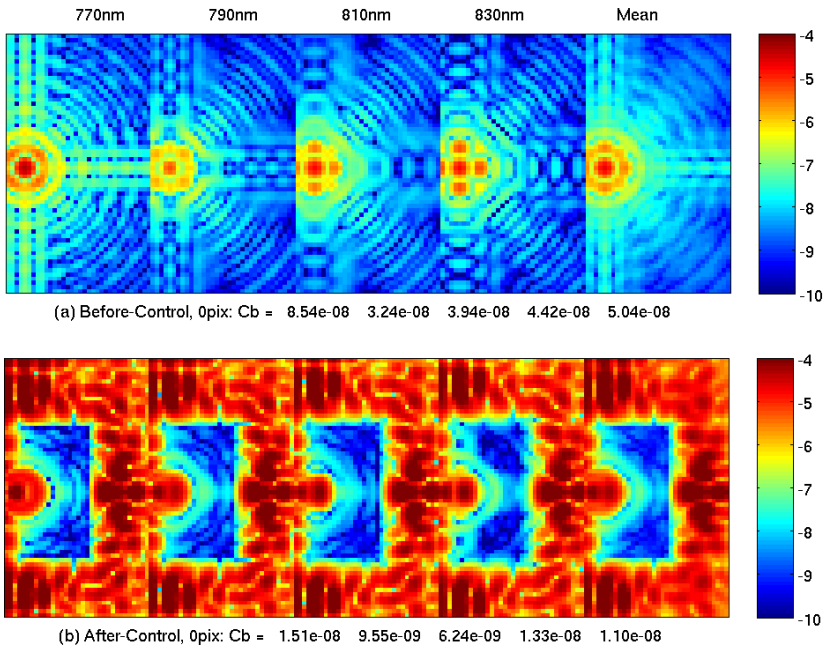

Fig.8. Contrast maps at four individual wavelengths, 770, 790, 810 and 830nm, and their mean. (a) Before-control, and (b) after broadband-control corresponding to a Lyot stop whose clear aperture is not reduced. The x-label of each panel lists the C_b –values at the four different wavelengths and that corresponding to 10%-broadband. The image corresponding to each wavelength extends from -1 to +10 $(\lambda/D)_{sky}$ in both *x* and *y*.

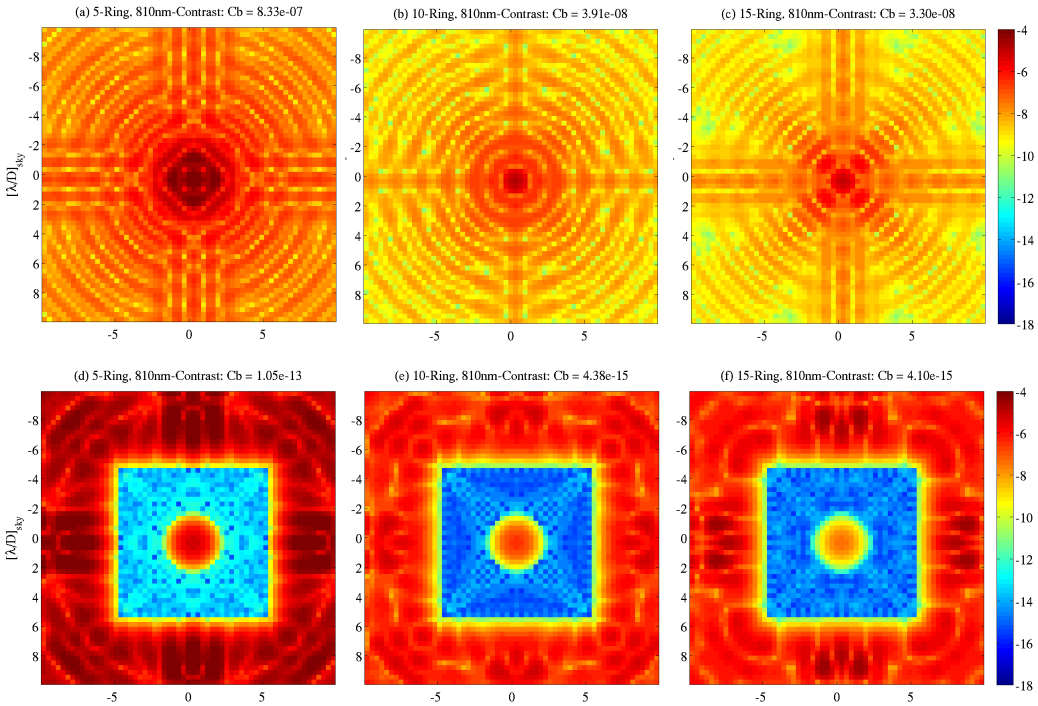

Fig.9. (a)-(c) Before-control contrast maps at the wavelength λ = 810nm obtained with the 5-, 10- and 15-ring occulting masks. (d)-(f) After-control contrast maps correspond to parts (a)-(c). The image corresponding to each case extends from -10 to +10 $(\lambda/D)_{sky}$ in both *x* and *y*.

of λ = 800nm, and the resulting DM solutions were evaluated with 10%-broadband light, we obtained a broadband mean contrast value of 4.14E-8. Decreasing the opening of the Lyot stop made the broadband contrast value worse. We have also designed other three occulting masks having 5-ring, 10-ring and 15-ring dielectric layers, based only on monochromatic considerations, and evaluated their monochromatic and broadband contrast performance. The resulting monochromatic mean contrast values are 1.05E-13, 4.38E-15, and 4.10E-15, respectively, while the broadband control and evaluation produced mean contrast values of 3.93E-6, 2.03E-6, and 1.06E-6, respectively.

These results point to an increased reliance on further optimization of the broadband mask design, or on an as-yet-unidentified architecture change, for improved overall performance of PIAACMC, as opposed to reliance on broadband wavefront control. The broadband mask optimization clearly has a strong impact on the broadband performance, resulting in nearly 50× better contrast of the 20-ring mask (which was partially optimized for broadband performance) compared to the 5, 10, and 15-ring masks (which included no broadband consideration in their design).

ACKNOWLEDGEMENTS

This work was carried out at the Jet Propulsion Laboratory, California Institute of Technology, under contract with the National Aeronautics and Space Administration.

REFERENCES

[1] Guyon, O. et al., "High-contrast imaging and wavefront control with a PIAA coronograph: Laboratory system validation,", Pub. Astron. Soc. Pacific 122, 71-84 (2010).
[2] Guyon O. et al., "Phase induced amplitude apodization (PIAA) coronagraphy: recent results and future prospects," *Proc. SPIE*, **8151**, 81510H (2011).
[3] Guyon O. et al., "Phase induced amplitude apodization (PIAA) coronagraphy: recent results and future prospects," *Proc. SPIE*, **8442**, 84424V (2012).
[4] Erkin Sidick, Brian Kern, Andreas Kuhnert, and Stuart Shaklan, "Comparison of Simulated Contrast Performance of Different Phase Induced Amplitude Apodization (PIAA) Coronagraph Configurations," *Proc. SPIE*, 8841, pp.88641Y (2013).
[5] Kern, B. et al., "Phase-induced amplitude apodization (PIAA) coronagraph testing at the High Contrast Imaging Testbed," *Proc. SPIE*, **7440**, 7440H (2009).
[6] Belikov, R. et al., "EXCEDE technology development I: First demonstration of high contrast at 1.2 lambda/D for an Explorer space telescope mission," *Proc. SPIE* **8442**, 844209 (2012).
[7] Erkin Sidick, Stuart Shaklan, and Kunjithapatham Balasubramanian, "HCIT broadband contrast performance sensitivity studies," *Proc. SPIE,* **8520**, pp.85200M (2012).
[8] Erkin Sidick, Scott A. Basinger, and David C. Redding, "An improved wavefront control algorithm for large space telescopes," *Proc. SPIE*, **7015**, 70154P (2008).
[9] Amir Give'on *et al.*, "Broadband wavefront correction algorithm for high-contrast imaging system," *Proc. SPIE*, **6691**, 66910A (2007).